Philosophical Magazine, 11 December 2004
Vol. 84, No. 35, 3785–3801

Taylor & Francis
Taylor & Francis Group

Negative stiffness-induced extreme viscoelastic mechanical properties: stability and dynamics

Yun-Che Wang and Roderic Lakes†

Department of Engineering Physics, Engineering Mechanics Program, University of Wisconsin-Madison, 147 Engineering Research Building, 1500 Engineering Drive, Madison, WI 53706-1687, USA

[*Received 12 November 2003 and accepted in revised form 28 July 2004*]

Abstract

Use of negative stiffness inclusions allows one to exceed the classic bounds upon overall mechanical properties of composite materials. We here analyse discrete viscoelastic 'spring' systems with negative stiffness elements to demonstrate the origin of extreme properties, and analyse the stability and dynamics of the systems. Two different models are analysed: one requires geometrical nonlinear analysis with pre-load as a negative stiffness source and the other is a linearized model with a direct application of negative stiffness. Material linearity is assumed for both models. The metastability is controlled by a viscous element. In the stable regime, extreme high mechanical damping $\tan\delta$ can be obtained at low frequency. In the metastable regime, singular resonance-like responses occur in $\tan\delta$. The pre-stressed viscoelastic system is stable at the equilibrium point with maximal overall compliance and is metastable when tuned for maximal overall stiffness. A reversal in the relationship between the magnitude of complex modulus and frequency is also observed. The experimental observability of the singularities in $\tan\delta$ is discussed in the context of designed composites and polycrystalline solids with metastable grain boundaries.

§ 1. Introduction

Negative stiffness inclusions have been used to achieve extreme high stiffness and high damping composites as demonstrated experimentally and analysed recently (Lakes 2001a,b, Lakes *et al.* 2001, Wang and Lakes 2004a,b). Anomalies in material modulus and damping, due to negative stiffness enhancement, are theoretically reported for Reuss-type composites (Lakes 2001a), and isotropic two-phase composites (Lakes 2001b). Through the formulas for calculating effective modulus and the elasticity-viscoelasticity correspondence principle for obtaining effective viscoelastic properties of composites, Lakes and his colleagues have theoretically shown the possibilities to exceed conventional bounds, which were articulated by Paul (1960) and Hashin and Shtrikman (1963), in materials' mechanical properties. Experimental verifications have also been reported via a buckled rubber tube (Lakes 2001a), as an example of Reuss-type composites, and VO_2-Sn composite system (Lakes *et al.* 2001), as an example of Hashin-Shtrikman composites. In addition to unusual mechanical properties, many anomalies in coupled field responses,

† Author for correspondence. Email: lakes@engr.wisc.edu.

Philosophical Magazine ISSN 1478–6435 print/ISSN 1478–6443 online
http://www.tandf.co.uk/journals
DOI: 10.1080/1478643042000282702

such as thermal expansion coefficients, piezoelectric coefficients, pyroelectric coefficients, or electric permittivities, have also been theoretically discussed in Wang and Lakes (2001). The causal mechanism for the phenomena is due to the interplay between the contributions from negative stiffness and positive stiffness phases.

Negative stiffness is different from negative Poisson's ratio in that stiffness and Poisson's ratio are two independent parameters for a homogeneous and isotropic material. Negative stiffness entails a reversal relationship between load and displacement for conventional, deformable materials. Poisson's ratio, denoted as ν, is defined as the negative lateral strain of a stressed body divided by its longitudinal strain. Based on the assumption of positive definiteness of strain energy, the range of the Poisson's ratio for isotropic solids is from -1 to 0.5, which implies stability. Therefore, although negative Poisson's ratio materials are uncommon, they are stable, whereas negative stiffness bulk materials are unstable. Recently, negative Poisson's ratio foams with ν as small as -0.8 (Lakes 1987, 1993a) have been fabricated and analysed. We remark that most solid materials have a Poisson's ratio between 0.25 and 0.33. The stiffness of these foams is nevertheless positive. It is understood that negative stiffness elastic systems, which are unstable, cannot exist any longer than an infinitesimal time period before they change their geometrical shape (on a microscopic or macroscopic scale) to a nearby stable equilibrium point.

The stability of systems with a negative stiffness element is intriguing. A bulk solid of negative stiffness materials is unquestionably unstable, but if all of its boundaries are fully constrained in displacement control, it can be stable, in which stability requires shear modulus (G) and Poisson's ratio (ν) to be $G>0$ and $-\infty<\nu<0.5$ or $1<\nu<\infty$ (Bramble and Payne 1963). Since Young's modulus is $E=2G(1+\nu)$ for isotropic homogeneous materials, the Young's modulus can legitimately be negative for constrained solids. Furthermore, if the condition of strong ellipticity, $G>0$ and $\nu<0.5$ or $\nu>1$, is satisfied, isotropic and homogeneous materials can have negative bulk and Young's modulus without losing uniqueness in their elasticity solutions (Knowles and Sternberg 1978) under no restrictions on boundary condition. Also, it implies real waves can propagate in the media. However, these criteria are only valid for homogeneous materials comprised of a single constituent. Lakes and Drugan (2002) demonstrated that Reuss-type composites with negative stiffness inclusions are unstable, based on an energy argument in the linear elasticity context. Instead of investigating the stability problem through the viewpoint of continuum mechanics, Wang and Lakes (2003, 2004a) investigated discrete, pre-stressed spring models, and showed that the system can exhibit extreme effective stiffness with the aid of a pair of pre-stressed springs as a negative stiffness element under a quasi-static assumption. They established a preliminary link between stabilized negative stiffness and pre-load. Their stability analysis was performed based on Lyapunov's indirect stability theorem, and they showed that systems of this sort are stable at the equilibrium point for extreme high overall compliance, metastable for extreme high stiffness, as well as stable for extreme high overall damping.

The objective of this paper is to analyse the stability and low-frequency dynamics of viscoelastic "spring" systems with negative stiffness components. We first lay down the mathematical foundation for solving the dynamical systems and related stability theories. Then, we perform parametric analysis, and discuss the implications of our numerical study in the context of experimental observation of high damping or sharp peaks in the damping of polycrystalline media.

§ 2. Analysis

2.1. *Viscoelastic geometric nonlinear analysis*

In this section, we derive the governing equations for the viscoelastic system shown in figure 1(a) with viscoelastic elements and pre-load, and its stability. The pre-loads are denoted as F_1^0, F_2^0 and F_3^0. The symbol θ (not shown in the diagram due to $\theta = 0$) and ϕ indicate the initial angle of the element bc and ac, respectively, with respect to the vertical line cd, respectively. k_1, k_2 and k_3 are spring constants, and $t_{\varepsilon j}$ and $t_{\sigma j}$ are the time constants for a standard linear solid for the j-th element, where $j = 1, 2, 3$. m_a and m_b are the masses at points a and b, respectively. The generalized coordinates α and β will be used as primary variables to analyse the problem. This model is adopted to demonstrate anomalies in effective properties for systems with negative stiffness components. Viscoelastic properties and dynamic responses of systems of this sort will be analysed by using a different model later. The relation between pre-stress and negative stiffness has been reported elsewhere, for example Wang and Lakes (2004a) and Iesan (1989). Figure 1(b) is a possible generalization for a two-dimensional lattice structure. In the following, we first present the constitutive model for characterizing a viscoelastic element, kinematic relations between deformation and displacement, and then force balancing relations.

As for the constitutive relationship, the standard linear solid model (Zener 1948) is adopted for all the "spring" elements, due to its mathematical simplicity and frequency dependence to reflect somewhat realistic materials. The structure of each element as a composite of elastic springs and a viscous dashpot is shown in the inset diagram in figure 1(a). The viscoelastic properties are to be the control parameters in the analysis of the stability of the model at equilibrium positions. The constitutive equations for each of the viscoelastic "springs", indicated by subscripts or superscripts 1, 2 and 3, in the system can be written as follows:

$$F_1 + \tau_\varepsilon^1 \dot{F}_1 = k_1\left(\Delta_1 + \tau_\sigma^1 \dot{\Delta}_1\right) + F_1^0, \tag{1}$$

$$F_2 + \tau_\varepsilon^2 \dot{F}_2 = k_2\left(\Delta_2 + \tau_\sigma^2 \dot{\Delta}_2\right) + F_2^0, \tag{2}$$

$$F_3 + \tau_\varepsilon^3 \dot{F}_3 = k_3\left(\Delta_3 + \tau_\sigma^3 \dot{\Delta}_3\right) + F_3^0, \tag{3}$$

where

$$\Delta_1 = \frac{h}{\cos(\theta - \alpha)} - \frac{h}{\cos\theta}, \tag{4}$$

$$\Delta_2 = (h\tan(\phi - \beta) - h\tan(\theta - \alpha)) - (h\tan\phi - h\tan\theta), \tag{5}$$

$$\Delta_3 = \frac{h}{\cos(\phi - \beta)} - \frac{h}{\cos\phi}. \tag{6}$$

Here, F's are the total internal forces in the springs. Equations (4)–(6) are the kinematic relations between deformation (Δ) of springs and the generalized coordinates, derived by inspection. In the standard linear solid model, the symbol k represents the relaxed spring constant. In equations (1)–(3), the static stiffness does not change with the time constants. Also, assuming τ_εs and τ_σs to be zero leads to the purely elastic material model. For a standard linear solid, passive viscoelastic systems require that τ_σ is greater than τ_ε to ensure damping $\tan\delta$ greater than 0. A

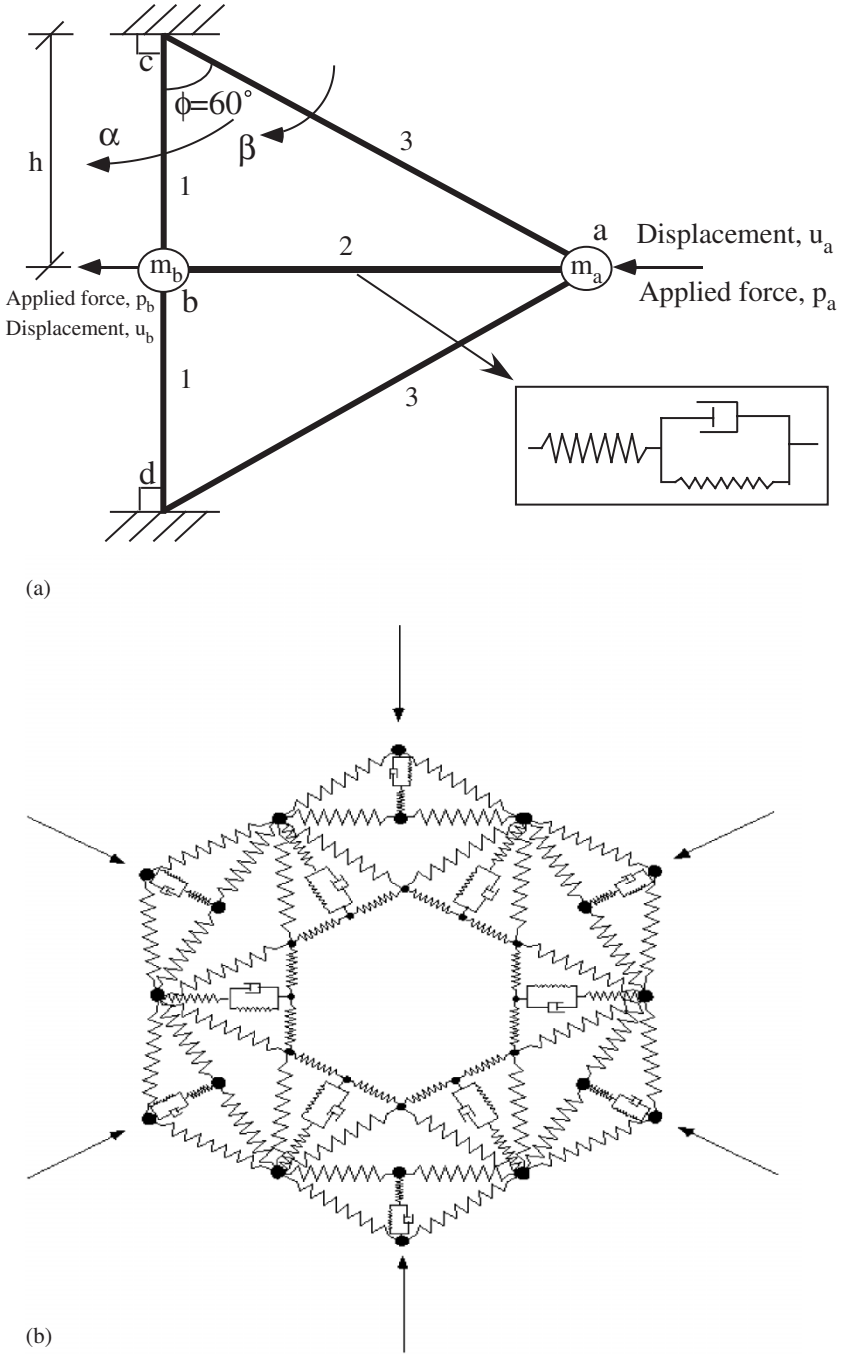

Figure 1. (a) 2D viscoelastic "spring" system with negative stiffness components embedded when compressional pre-load is assigned in the bc and bd element (number 1). The spring constants are pre-chosen: $k_1 = 10$, $k_2 = 3$ and $k_3 = 5\,\mathrm{kN/m}$. p_b is always set to zero. (b) A proposed lattice structure assembled with the building block shown in (a) with only the ab element being viscoelastic.

typical solution of the ordinary differential equation of this kind in time domain is found as follows:

$$F_j(t) = e^{(-1/\tau_\varepsilon^j)t}\left\{\int_0^t \frac{1}{\tau_\varepsilon^j}\left(k_j\Delta_j + k_j\tau_\sigma^j\dot{\Delta}_j + F_j^0\right)e^{(-1/\tau_\varepsilon^j)t}dt + c_j\right\}. \tag{7}$$

Here $j = 1$, 2, or 3, for labelling springs and c_j is an integration constant, determined by initial conditions of Δj, i.e. $c_j = (k_j\tau_\sigma^j/\tau_\varepsilon^j)\Delta_j|_{t=0}$.

The Newtonian equations of motion are as follows:

$$m_a\ddot{u}_a = p_a + F_2 + 2F_3\sin(\phi - \beta), \tag{8}$$

$$m_b\ddot{u}_b = 2F_1\sin(\theta - \alpha) - F_2, \tag{9}$$

where

$$u_a = h\tan\,\phi - h\tan(\phi - \beta), \tag{10}$$

$$u_b = h\tan\theta - h\tan(\theta - \alpha). \tag{11}$$

By substituting kinematic relations to equations (4) and (6), the equations of motion can be expressed as follows in terms of the generalized coordinates.

$$\mathbf{A}\begin{Bmatrix}\ddot{\alpha}\\ \ddot{\beta}\end{Bmatrix} + \mathbf{B}\begin{Bmatrix}\dot{\alpha}^2\\ \dot{\beta}^2\end{Bmatrix} = \begin{Bmatrix}2F_1(t)\sin(\theta - \alpha) - F_2(t)\\ p_a + F_2(t) + 2F_3(t)\sin(\phi - \beta)\end{Bmatrix}, \tag{12}$$

where

$$\mathbf{A} = \begin{bmatrix} m_b h\sec^2(\theta - \alpha) & 0\\ 0 & m_a h\sec^2(\phi - \beta)\end{bmatrix}, \tag{13}$$

$$\mathbf{B} = \begin{bmatrix} -2m_b h\sec^2(\theta - \alpha)\tan(\theta - \alpha) & 0\\ 0 & -2m_a h\sec^2(\phi - \beta)\tan(\phi - \beta)\end{bmatrix}. \tag{14}$$

Importing the solution, equation (7), into the equations of motion, equations (12)–(14), will lead to an integro-differential type of governing equation. To avoid the difficulty of solving this type of equation and facilitate the stability analysis, the state-space technique (Meirovitch 1970) is used to reduce equations (12)–(14) to first-order ODE's. Incorporating the constitutive equations, the equations, which govern the "spring" system, can be expressed as a first order ODE system with the state-space variables α, β, w, v, F_1, F_2, and F_3, in the form of

$$\mathbf{M}\dot{\mathbf{x}} = \mathbf{X}(\mathbf{x}), \tag{15}$$

where

$$\mathbf{x} = \begin{bmatrix}\dot{\alpha} & \dot{\beta} & \dot{w} & \dot{v} & \dot{F}_1 & \dot{F}_2 & \dot{F}_3\end{bmatrix}^{\mathrm{T}}, \tag{16}$$

$$\mathbf{M} = \begin{bmatrix} 1 & 0 & 0 & 0 & 0 & 0 & 0\\ & 1 & 0 & 0 & 0 & 0 & 0\\ & & m_b h\sec^2(\theta - \alpha) & 0 & 0 & 0 & 0\\ & & & m_a h\sec^2(\phi - \beta) & 0 & 0 & 0\\ & & & & \tau_\varepsilon^1 & 0 & 0\\ & \text{sym.} & & & & \tau_\varepsilon^2 & 0\\ & & & & & & \tau_\varepsilon^3\end{bmatrix}, \tag{17}$$

$$\mathbf{X} = \begin{Bmatrix} w \\ v \\ 2m_b h \sec^2(\theta-\alpha)\tan(\theta-\alpha)w^2 + 2F_1 \sin(\theta-\alpha) - F_2 \\ 2m_a h \sec^2(\phi-\beta)\tan(\phi-\beta)v^2 + 2F_3 \sin(\phi-\beta) + F_2 + p_a \\ -F_1 + k_1\left(\Delta_1 + \tau_\sigma^1 \dot{\Delta}_1\right) + F_1^0 \\ -F_2 + k_2\left(\Delta_2 + \tau_\sigma^2 \dot{\Delta}_2\right) + F_2^0 \\ -F_3 + k_3\left(\Delta_3 + \tau_\sigma^3 \dot{\Delta}_3\right) + F_3^0 \end{Bmatrix}. \tag{18}$$

T denotes the transpose operator in matrix theory. The variables w and v are the generalized velocities for α- and β-coordinates, respectively. So $w = \dot{\alpha}$ and $v = \dot{\beta}$. The equations of motion in the state-space representation, as above, are desirable for stability analysis (Leipholz 1980, 1987, Strogatz 1994). It is noted that to facilitate the later numerical study of the equations, we define $r_j = \tau_{\sigma j}/\tau_{\varepsilon j}$, for the j-th spring element. The physical meaning of r_j is directly related to the relaxation strength, Λ, which is defined as the ratio of the difference between unrelaxed and relaxed modulus to relaxed modulus (Zener 1948), as follows:

$$\Lambda_j = r_j - 1, \quad j = 1, 2, 3. \tag{19}$$

The equations derived here are valid for all elements to be viscoelastic and prestressed. However, to simplify later numerical analysis, and demonstrate the essential features of the system, we limit ourselves to have $r_1 = r_3 = 0$, and $F_2^0 = F_3^0 = 0$ so that elements 1 and 3 are elastic and only element 2 is viscoelastic. Therefore, we define a viscoelastic parameter for the k_2 element as $r = \tau_{\sigma 2}/\tau_{\varepsilon 2}$, and consequently $\eta = k_2 \tau_{\varepsilon 2}$ $(r + r/(r-1))$. Hence, F_1^0 and r are the tuning parameters for negative stiffness and degree of stability, respectively, and will be intensively used later.

The above equations involving viscoelastic effects can be reduced to equations for purely elastic cases by letting all of the time constants be zero. After doing so and re-arranging equations in equations (12) and (14) with equations (1)–(3) to eliminate internal forces, Fs, one obtains the equations of motion for the elastic system (Wang and Lakes 2004a) without damping effects as follows.

$$\mathbf{A}\begin{Bmatrix} \ddot{\alpha} \\ \ddot{\beta} \end{Bmatrix} + \mathbf{B}\begin{Bmatrix} \dot{\alpha}^2 \\ \dot{\beta}^2 \end{Bmatrix} = \begin{Bmatrix} \dfrac{2k_1 h \sin(\theta-\alpha)}{\cos(\theta-\alpha)} - \dfrac{2k_1 h \sin(\theta-\alpha)}{\cos\theta} + 2F_1^0 \sin(\theta-\alpha) \\ -\left[k_2(h\tan(\phi-\beta) - h\tan(\theta-\alpha) - h\tan\phi + h\tan\theta) + F_2^0\right] \\ p_a + \left[k_2(h\tan(\phi-\beta) - h\tan(\theta-\alpha) - h\tan\phi + h\tan\theta) + F_2^0\right] \\ \quad + \dfrac{2k_3 h \sin(\phi-\beta)}{\cos(\phi-\beta)} - \dfrac{2k_3 h \sin(\phi-\beta)}{\cos\phi} + 2F_3^0 \sin(\phi-\beta) \end{Bmatrix} \tag{20}$$

where

$$\mathbf{A} = \begin{bmatrix} m_b h \sec^2(\theta-\alpha) & 0 \\ 0 & m_a h \sec^2(\phi-\beta) \end{bmatrix}, \tag{21}$$

$$\mathbf{B} = \begin{bmatrix} -2m_b h \sec^2(\theta-\alpha)\tan(\theta-\alpha) & 0 \\ 0 & -2m_a h \sec^2(\phi-\beta)\tan(\phi-\beta) \end{bmatrix}. \tag{22}$$

2.2. *Linear analysis with negative stiffness*

In the previous section, we established the mathematical foundation for studying the negative stiffness effect by using pre-stressed spring elements with the consideration of geometric nonlinear effects. The equivalence of using pre-stressed elements with a unique geometry and allowing stiffness to be negative has been established in Wang and Lakes (2004a). The system in figure 2 is constructed to contain elements of both negative and positive stiffness, to have an equilibrium configuration at zero applied load, and to contain a damping element to confer metastability. The system chosen has no more complexity than is needed to achieve these characteristics.

Therefore, in this section, we derive governing equations to analyse the geometrically linear, viscoelastic spring model in figure 2 with the allowance of κ_1 to be negative to show complicated and interesting phenomena in the dynamics and stability of this sort of system. The rationale for studying this model is to simplify the mathematical complexity involved in the previous section, yet preserve the essential feature of a system with a negative stiffness inclusion. The governing equations of the system are readily written as follows, with $F_1 = 0$ throughout the analysis to simulate usual two-phase composite materials with no external forces applied at their interfacial boundaries:

$$\begin{bmatrix} m_1 & 0 \\ 0 & m_2 \end{bmatrix} \begin{pmatrix} \ddot{u}_1 \\ \ddot{u}_2 \end{pmatrix} + \begin{bmatrix} k_1 + k_2 & -k_2 \\ -k_2 & k_2 \end{bmatrix} \begin{pmatrix} u_1 \\ u_2 \end{pmatrix} + \begin{pmatrix} f \\ 0 \end{pmatrix} = \begin{pmatrix} 0 \\ F_2 \end{pmatrix}, \tag{23}$$

$$f + \frac{\eta}{\kappa_1 + \kappa_2} \dot{f} = \frac{\kappa_1 \kappa_2}{\kappa_1 + \kappa_2} u_1 + \frac{\kappa_1 \eta}{\kappa_1 + \kappa_2} \dot{u}_1. \tag{24}$$

Here f is the internal force in the standard linear solid module, composed of the spring elements κ_1 and κ_2, and the dashpot element η. The symbol η denotes viscosity, and k's and κ's spring constants. The overall loss tangent is easier to compute in the frequency domain with the aid of the Fourier transformation of equations (23) and (24), as follows:

$$\begin{bmatrix} -\omega^2 m_1 + k_1 + k_2 + \dfrac{\kappa_1 \kappa_2 + i\omega\kappa_1\eta}{\kappa_1 + \kappa_2 + i\omega\eta} & -k_2 \\ -k_2 & -\omega^2 m_2 + k_2 \end{bmatrix} \begin{pmatrix} \tilde{u}_1 \\ \tilde{u}_2 \end{pmatrix} = \begin{pmatrix} 0 \\ \tilde{F}_2 \end{pmatrix}. \tag{25}$$

Here the tilde denotes the Fourier-transformed variables. Assigning $\omega = 0$, one can obtain the compliance of the system at the low frequency limit (i.e. quasi-static

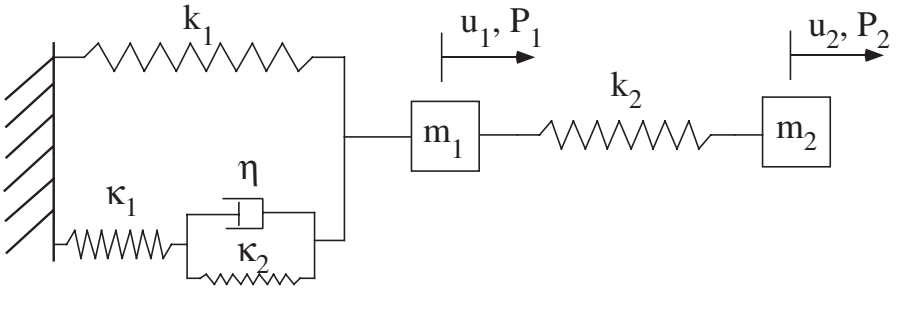

Figure 2. Linearized spring-damper model for exploring the stability and frequency response of extreme high damping due to negative κ_1. $k_1 = 10$, $k_2 = 5$ and $\kappa_2 = 5\,\mathrm{kN/m}$ are fixed in analysis. Tuning parameters are κ_1 and η. $P_1 = 0$ throughout.

processes). At a specific ω, the effective dynamic compliance, j_{eff}, and the overall loss tangent of the system, $\tan\delta$, are as follows:

$$j_{\text{eff}} = \left|\tilde{u}_2/\tilde{F}_2\right|, \tag{26}$$

$$\tan\delta = \frac{\text{Im}\left(\tilde{F}_2/\tilde{u}_2\right)}{\text{Re}\left(\tilde{F}_2/\tilde{u}_2\right)}. \tag{27}$$

For the stability of the system in the sense of Routh-Hurwitz, the governing equations, equations (23) and (24), are rewritten in state space, as follows.

$$\mathbf{M}\begin{pmatrix}\dot{u}_1\\ \dot{u}_2\\ \dot{v}_1\\ \dot{v}_2\\ \dot{f}\end{pmatrix} = \mathbf{K}\begin{pmatrix}u_1\\ u_2\\ v_1\\ v_2\\ f\end{pmatrix} + \begin{pmatrix}0\\ 0\\ 0\\ F_2\\ 0\end{pmatrix}, \tag{28}$$

where

$$\mathbf{M} = \begin{bmatrix} 1 & 0 & 0 & 0 & 0\\ & 1 & 0 & 0 & 0\\ & & m_1 & 0 & 0\\ & \text{sym.} & & m_2 & 0\\ & & & & \eta \end{bmatrix}, \quad \text{and} \tag{29}$$

$$\mathbf{K} = \begin{bmatrix} 0 & 0 & 1 & 0 & 0\\ 0 & 0 & 0 & 1 & 0\\ -(k_1+k_2) & k_2 & 0 & 0 & -1\\ k_2 & -k_2 & 0 & 0 & 0\\ \kappa_1\kappa_2 & 0 & \kappa_1 & 0 & -(\kappa_1+\kappa_2) \end{bmatrix}. \tag{30}$$

The stability of this system will be investigated by discussing the eigenvalues of a $\mathbf{J}$ matrix, which is defined as $\mathbf{J} = \mathbf{M}^{-1}\mathbf{K}$ in this case.

2.3. *Stability*

For discrete autonomous dynamical systems, their governing equations can be expressed as follows.

$$\dot{x}_i = X_i(x_1, x_2, \ldots, x_m), \quad i = 1,2,\ldots,m. \tag{31}$$

Here if the systems are Hamiltonian with $H = H(q_k, p_k)$, $k = 1, 2, \ldots, n$, where n is the total number of degrees of freedom, then $m = 2n$, and $\mathbf{x}$ and $\mathbf{X}$ can be constructed as follows:

$$x_k = q_k, \quad x_n + k = p_k, \text{ and} \tag{32}$$

$$X_k = \partial H/\partial p_k, \quad X_{n+k} = -\partial H/\partial q_{n+k} \tag{33}$$

where

$$\dot{q}_k = \frac{\partial H}{\partial p_k}, \quad \text{and} \quad \dot{p}_k = -\frac{\partial H}{\partial q_k}. \tag{34}$$

q_k and p_k are generalized coordinates and generalized momenta, respectively. Therefore, the physical meaning of the variables is clear. $\mathbf{x}$ is a column vector containing the time-dependent generalized coordinates and momenta. $\mathbf{X}$ is a system-specific vector function, which can be determined with the Hamiltonian of the system. If the systems are non-Hamiltonian, such as dissipative systems, one still can construct the governing equations into the form, as equation (31), through Newton's second law and the state-space technique, which in essence reduces higher order differential equations to a system of first order differential equations. In this case, the physical meaning of the variables will be somewhat obscure. Also, it is not necessary for the dimension of equation (31), m, to be an even number. However, the methodology for stability analysis is unchanged, as follows.

Following the Lyapunov's theorem, or the so-called Routh-Hurwitz method (Meirovitch 1970, Leipholz 1980, 1987), the stability analysis of equation (31) is manifest at the eigenvalue analysis of the Jacobian matrix, defined as follows:

$$\mathbf{J} = \left.\frac{\partial \mathbf{M}^{-1}\mathbf{X}}{\partial \mathbf{x}}\right|_{\mathbf{x}=\mathbf{x}_e}, \tag{35}$$

where $\mathbf{x}$, $\mathbf{X}$ and $\mathbf{M}$ are defined in equations (16), (17) and (18), or (28), (29) and (30) for the two models, respectively. Note, for Hamiltonian systems, $\mathbf{M}$ is an identity matrix. The symbol $\mathbf{x}_e$ denotes the value of the state variables at equilibrium, which can be found by solving the algebraic equations, $\mathbf{X}(\mathbf{x}_e) = 0$. According to Lyapunov's indirect theorem for stability, at an equilibrium point, if $\mathbf{J}$ contains eigenvalues with no positive real parts, the system is stable infinitesimally around the equilibrium point. Strogatz (1994) points out that the stability of a dynamical system with zero real part in its eigenvalues is weak albeit stable. When all eigenvalues have negative real parts, the degree of stability can be understood as the distance between the imaginary axis and the closest eigenvalue in the complex plane for all the eigenvalues of the system (Leipholz 1987). Furthermore, the eigenvalue (λ), which has the smallest $|\mathrm{Re}(\lambda)|$, is responsible for the rate of decay (for $\mathrm{Re}(\lambda) < 0$) or growth (for $\mathrm{Re}(\lambda) > 0$) of vibration amplitudes in the system's normal modes. We remark that the conventional energy method (Wang and Lakes 2004a) is not suitable for the stability analysis of a dissipative system due to the changing in the energy landscape with respect to time (since mechanical energy is not conserved in such systems). Moreover Routh-Hurwitz criteria provide stability information by using only the algebraic relations between coefficients of the characteristic equation of the $\mathbf{J}$ matrix. Dorf (1992) uses an iteration scheme to discuss the stability of the system, which essentially predicts the same result as Routh-Hurwitz criteria. In our study, we exclusively analyse the eigenvalues with the aid of computation. Stability of the systems in figures 1(a) and 2 will be discussed in detail, based on Lyapunov's indirect method.

§ 3. Results and discussion

The elastic counterparts of the mechanical properties of figure 1 have been reported in Wang and Lakes (2004a). We here investigate the similar system with the consideration of viscoelastic effects. The spring constants are pre-chosen: $k_1 = 10$, $k_2 = 3$, and $k_3 = 5\,\mathrm{kN/m}$. The quasi-static assumption ($w = v = 0$) is used throughout. In figure 3(a), the effective absolute complex spring constant and the stability-losing eigenvalue, one of the eigenvalues of $\mathbf{J}$ matrix, calculated from equations (16), (17)

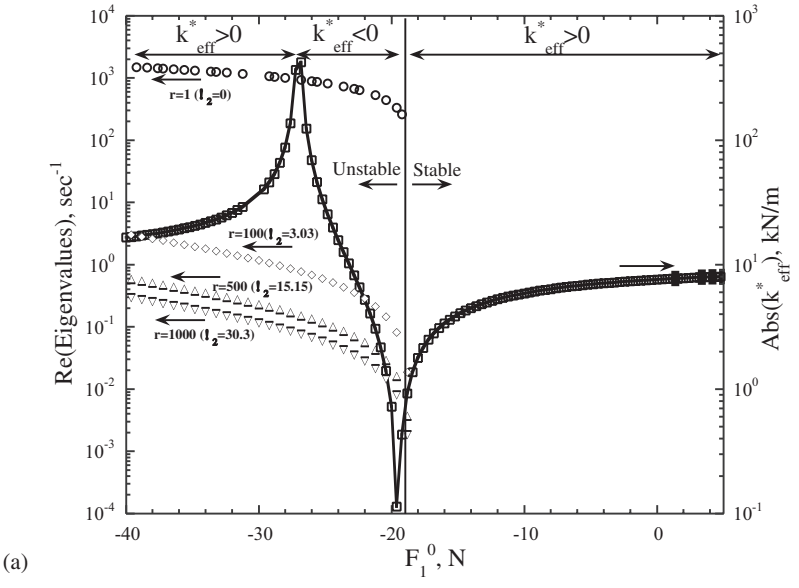

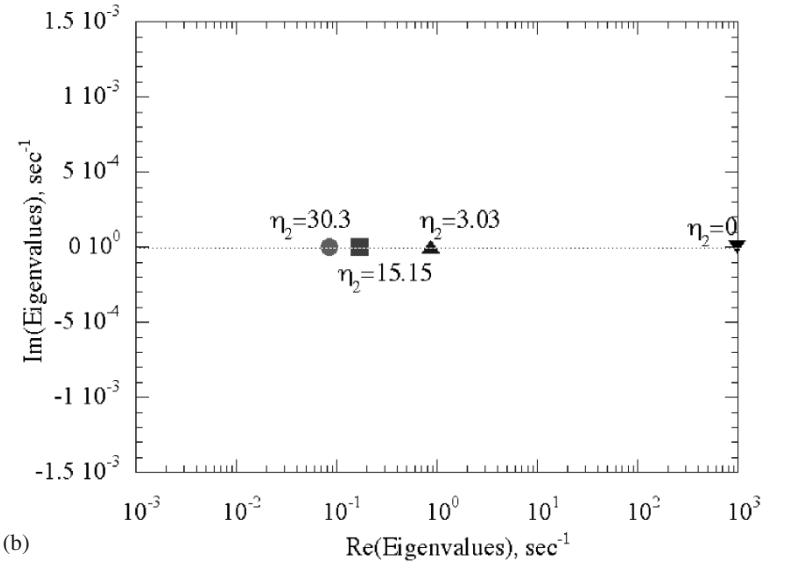

Figure 3. (a) Effective stiffness and the stability-losing eigenvalue vs. pre-stress (F_1^0) in the vertical springs in figure 1(a). The solid line was calculated from equation (20) for the purely elastic case, and the open square for the viscoelastic case with the quasi-static assumption, equation (15). The eigenvalues, calculated from equation (35) with equations (16)–(18), are negative for F_1^0 greater than about -19 N. The left scale shows the real part of the stability-losing eigenvalue. The right scale shows the effective stiffness or spring constant. Without pre-stress it is clearly stable, and has positive stiffness (7.5 kN/m). The regime with eigenvalues having positive real parts is unstable. The only damping element is in the k_2 element with $\tau_\varepsilon = 0.01$ throughout all the cases. (b) Root-locus plot of the system in figure 1(a) with $F_1^0 = -27.2$, $F_2^0 = 0$, and $F_3^0 = 0$ N. The tuning parameter is η, the viscous element parallel to the κ_2 spring. The trajectory of the eigenvalues indicates the system is metastable at the equilibrium point with extremely high stiffness.

and (18), are plotted versus the pre-load in F_1^0 As it can be seen, tuning pre-load changes the overall stiffness of the system dramatically. For the spring constant, the continuous solid curve is obtained from the purely elastic assumption, and the open square symbols represent the viscoelastic model, based on equation (15), for any r, defined as a measure of the viscoelasticity in equation (19). The coincidence of the two results is the consequence of the quasi-static assumption. It is noted, at $F_1^0 = -27.2\,\mathrm{N}$, with the pre-chosen resolution of 0.1 N increment on F_1^0in our calculations, the overall stiffness exhibits a thousand times increase, compared to the system with positive F_1^0. The resonance-like feature is the signature of the systems with negative stiffness elements, which has been observed previously (Lakes 2001a,b). Because of the quasi-static assumption (inertial terms are negligible) the observed sharp peaks are not resonant phenomena.

The magnitude of the stability-losing eigenvalue decreases with the increase of viscosity. This can be clearly seen on the root-locus plot, as shown in figure 3(b). The inverse of the eigenvalue is the divergence rate associated with instability. Therefore, the system is metastable at the equilibrium configuration with extreme high overall stiffness. The rate of divergence from equilibrium becomes slower as the viscosity η is increased. This is interpreted as follows. In spring-damper systems with positive spring constant k and viscosity η, the time constant for exponential decay of a perturbation is $\tau = \eta/k$. For an unstable system the effect of a perturbation grows with time, but it grows more slowly if the viscosity is large. Near the stability boundary, in the stable regime, the system exhibits extreme high overall compliance around $F_1^0 = -19\,\mathrm{N}$.

As for computational details for solving the geometrical nonlinear problem, we make the following remarks. For the purely elastic case, solving equation (20) with no dynamic effects is straightforward, in which one prescribes α to obtain β through the first equation of equation (20), p_a from the second equation, and u_a from equation (10). Then, one can obtain the load (p_a)–displacement (u_a) plots. However, it is not trivial to find equilibrium points for equation (15) since one needs to solve a nonlinear algebraic system with the five variables (β, F_1, F_2, F_3, and p_a), when α is prescribed. To ensure the convergence of the Newton-Raphson iteration method for solving the nonlinear system, the conventional incremental-iteration solution procedure (Bathe 1996) is adopted. During the calculation process, one incrementally prescribes α to calculate the unknown variables iteratively with initial guesses from the results of the calculation corresponding to the one-step previous α. Again, it is understood that the effective spring constant calculated from the viscoelastic model coincides with that from equation (20), since under the quasi-static assumption the dashpot does not contribute any resistant force.

As for the nature of a system of this kind, we remark that the mechanical system behaves in an extremely stiff (or compliant) manner when the inner springs contain compressional forces. Moreover, it is stable for extreme compliance, and metastable for extreme stiffness. If the vertical springs were isolated from the system, and contained stored compressional forces, the two-spring structure would not be stable since physically it is understood that any small perturbation will move the springs away from the vertical position (Wang and Lakes 2004a). Hence, the inner springs in figure 1(a) are named the negative stiffness element of the system. There are different types of negative stiffness elements, such as a buckled tube (Lakes 2001a) or materials undergoing phase transformation (Lakes *et al.* 2001). Nonetheless, these negative stiffness elements involve buckling on a macroscopic or microscopic scale.

Experimentally, embedding the negative stiffness elements into a matrix to form a composite has shown significant anomalies on damping and stiffness properties of materials (Lakes 2001a,b, Lakes *et. al.* 2001).

One can calculate overall damping of the above-mentioned system; however, the complexity involved due to the geometrical nonlinear effect is not trivial. Here, to simplify the analysis and illustrate the underlying physics, we analyse the linearized model in figure 2 allowing κ_1 to be negative for understanding its damping properties. The legitimacy of doing this is verified in Wang and Lakes (2004a). Wang and Lakes (2003) have reported that the system exhibits stable extreme (possibly singular) $\tan\delta$ with $\eta = 0.1\,\mathrm{kN\,m^{-1}\,s}$. Here, we conduct a more detailed study of this discrete system. In this model, the pre-chosen parameters are $m_1 = m_2 = 10^{-12}\,\mathrm{kg}$, $k_1 = 10$, $k_2 = 5$, $\kappa_2 = 5\,\mathrm{kN/m}$ and $\omega = 1\,\mathrm{rad/s}$. The results are shown in figure 4 with $\eta = 0.5\,\mathrm{kN\,m^{-1}\,s}$. Note that the system is unstable when $\kappa_1 < -3.34\,\mathrm{kN/m}$ due to the eigenvalue with a positive real part. It is noteworthy that no singularities are observed in $\tan\delta$ in this case. The mathematical analysis of the disappearance of the singularity can be found in Wang and Lakes (2003). In addition, the zero $\tan\delta$ at $\kappa_1 = 0$ is expected since the standard linear solid element is not physically connected to the left fixed end; thus, the whole system is purely elastic.

Furthermore, higher damping in the standard linear solid element reduces the magnitude of the anomaly in the absolute effective compliance of the system. To understand the effect of viscosity on the stability boundary, in figure 5, we plot

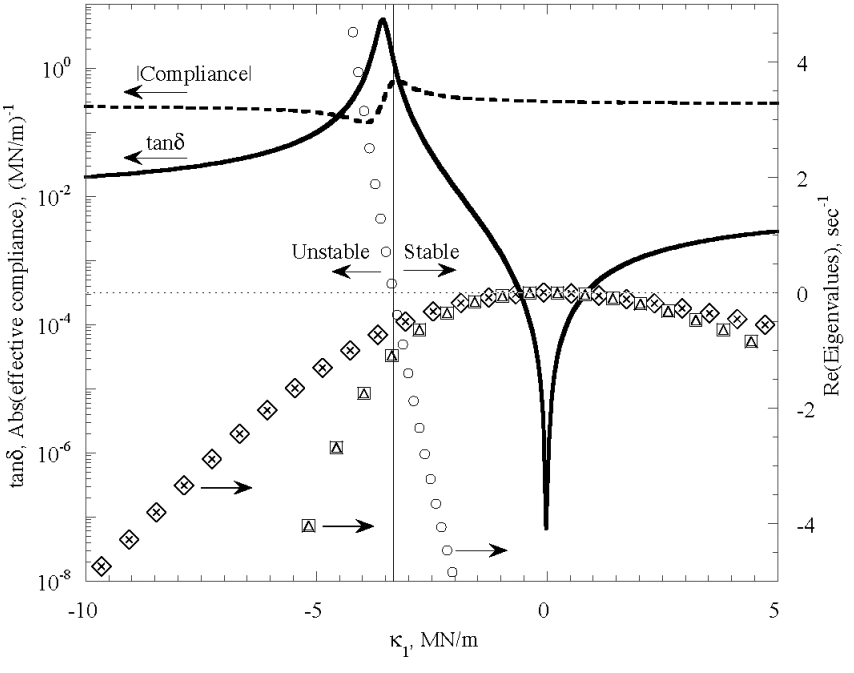

Figure 4. Stable high damping in a discrete system with pre-load. Compliance and $\tan\delta$ on a log scale (left axis), and real part of eigenvalues (open diamond, cross, open square, open triangle, and open circle) on a linear scale (right axis) versus κ_1 calculated from the model in figure 2, with $\eta = 0.5\,\mathrm{kN\,m^{-1}\,s}$. The fixed parameters are: $m_1 = m_2 = 10^{-12}\,\mathrm{kg}$, $k_1 = 10$, $k_2 = 5$, $\kappa_2 = 5\,\mathrm{kN/m}$, and $\omega = 1\,\mathrm{rad/s}$.

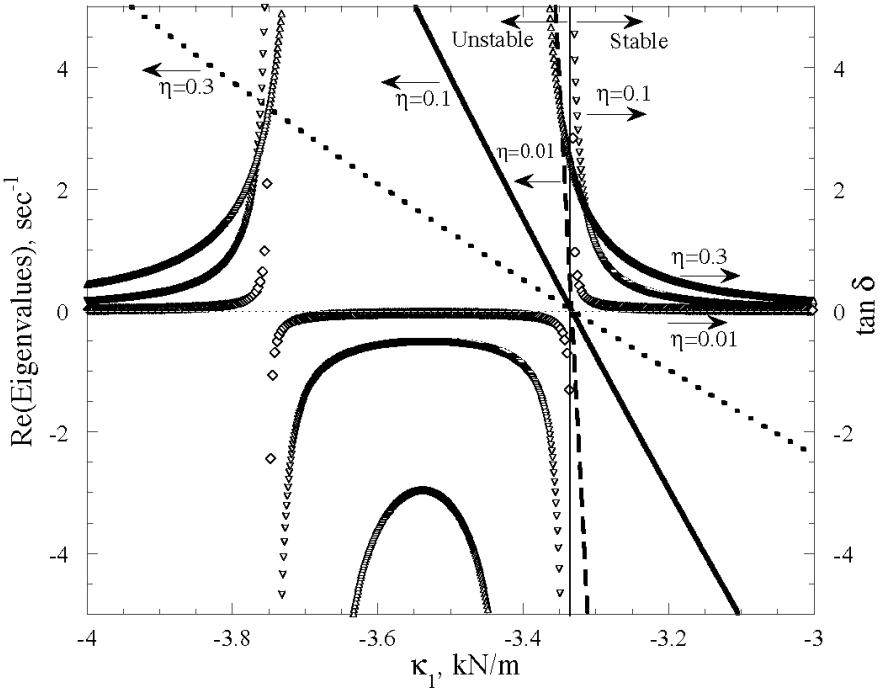

Figure 5. Tan δ and eigenvalues on a linear scale for $\eta = 0.01$, $\eta = 0.1$ and $\eta = 0.3\,\mathrm{kN\,m^{-1}\,s}$. The fixed parameters are: $m_1 = m_2 = 10^{-12}\,\mathrm{kg}$, $k_1 = 10$, $k_2 = 5$, $\kappa_2 = 5\,\mathrm{kN/m}$, and $\omega = 1\,\mathrm{rad/s}$.

$\tan\delta$ and the stability-losing eigenvalue with various viscosities with respect to κ_1. It is found that changing viscosity will not move the stability boundary, but will alter the asymptotic behaviour of the $\tan\delta$ versus negative stiffness. Also, the peak of $\tan\delta$ approaches the stability boundary as η decreases. Again, the magnitude of the positive real part eigenvalue decreases with the increase of viscosity, which indicates the metastability of the system.

The low frequency dynamic response of the system in figure 2 is presented in figure 6. We plot the overall $|\tan\delta|$ in figure 6(a) and $|k^*_{\mathrm{eff}}|$ in figure 6(b) with respect to sinusoidal driving frequency from 0.01 to 100 rad/s with $\eta = 0.1\,\mathrm{kN\,m^{-1}\,s}$. The stability boundary is found to be at $\kappa_1 = -3.3333\,\mathrm{kN/m}$. It is found, from stability analysis, regardless of driving frequency (far below any resonant frequency), that when $\kappa_1 < -3.3333\,\mathrm{kN/m}$, the system is metastable. In this regime, sharp peaks in the damping $\tan\delta$ can be observed. These peaks are not resonances since they occur at frequencies far below any natural frequency. Specifically, the structural resonant frequency of the system is typically about $10^6\,\mathrm{rad/s}$. To perform the calculations, non-zero mass must be assumed, but small node masses of $10^{-12}\,\mathrm{kg}$ are used, so that natural frequencies are far above the frequency range of interest.

In the stable regime, i.e. $\kappa_1 > -3.3333\,\mathrm{kN/m}$, one can see humps in the damping, similar to the well-known Debye peaks. Also, as noticed, the corresponding curves of the dynamic spring constant in figure 6(b) do not exhibit resonance-like features. The stability-related eigenvalue, λ, plotted where $\lambda < 0$ indicates stability and $\lambda > 0$ metastability. Other eigenvalues have been checked to have no positive real parts.

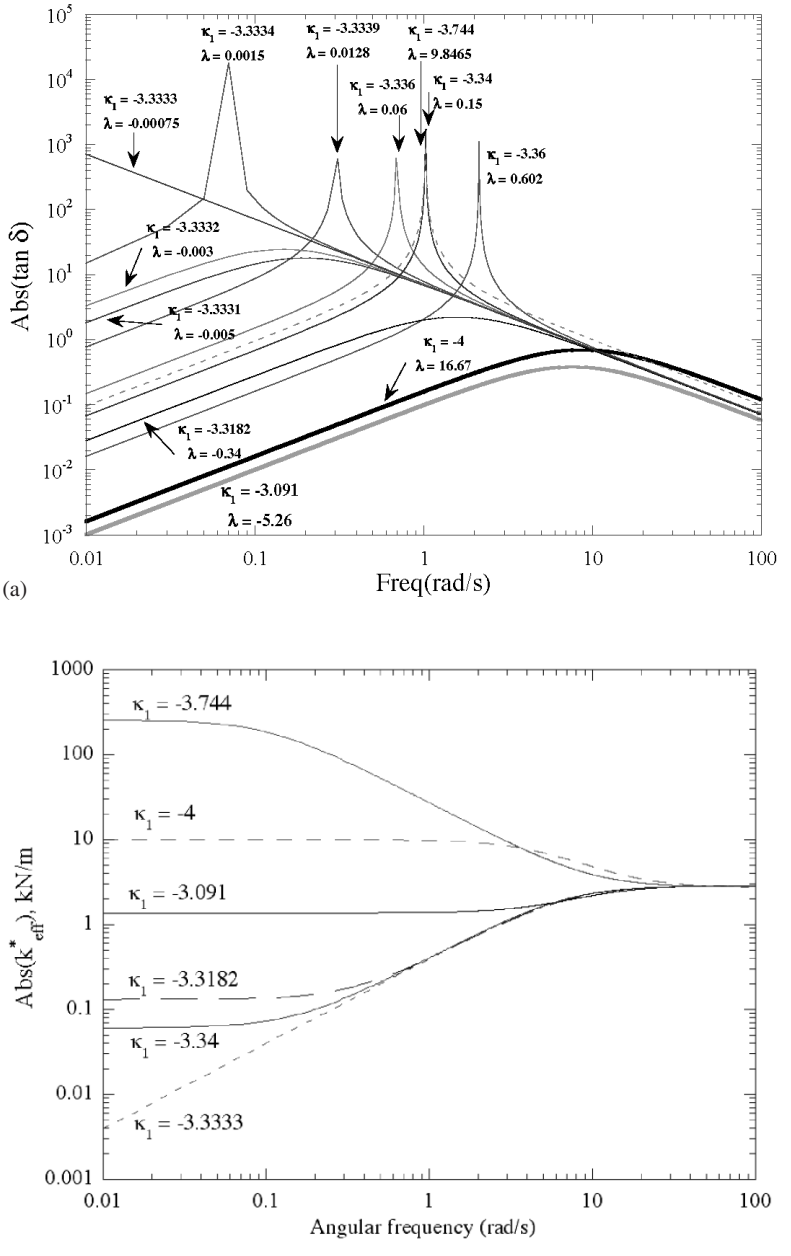

Figure 6. Low-frequency response of the absolute value of (a) loss tangent and (b) absolute value of the dynamic modulus of the system, shown in figure 2. The symbol, λ, represents the stability-losing eigenvalue in units of second^{-1}. $\eta = 0.1\,\mathrm{kN\,m^{-1}\,s}$ for all curves. For $\kappa_1 > -3.3333\,\mathrm{kN/m}$, the loss tangent is greater than zero, and for $\kappa_1 < -3.3333\,\mathrm{kN/m}$, the left side of a sharp peak is negative, and the right side is positive. At the stability boundary, $\kappa_1 = -3.3333\,\mathrm{kN/m}$, the slope of the $\tan\delta$ curve versus frequency is about -1. The sharp peaks indicate the singularities in $\tan\delta$. The humps in $\tan\delta$ are similar to Debye peaks. The reversal of frequency dependence of the dynamic spring constant is observed when the negative stiffness is suitably tuned. The eigenvalue analysis reveals the system is unstable when $\kappa_1 < -3.3333\,\mathrm{kN/m}$.

The metastable system has a higher divergent rate (i.e. the inverse of λ) when κ_1 is more negative. The rate of divergence (λ) is correlated with elemental characteristic time constants as follows (Wang and Lakes 2003). $\lambda = -(1/\tau_c + 1/\tau_\sigma)$, where $\tau_c = \eta/k_c$, $1/k_c = 1/k_1 + 1/\kappa_1$, and $\tau_\sigma = \eta/\kappa_2$. In this parametric study, since η and κ_2 are prechosen, respectively, to be $0.1\,\mathrm{kN\,m^{-1}\,s}$ and $5\,\mathrm{kN/m}$, $\tau_\sigma = 0.02\,\mathrm{s}$ throughout. Therefore, the rate of divergence is determined mainly by the interplay between k_1 and κ_1. Moreover, the asymptotic slope (on a log–log scale) of the $\tan\delta$ curve at high frequency (greater than 100 rad/s and less than the structural resonant frequency) is about -1 for all studied cases. The rationale is the high frequency response of a standard linear solid is not dominated by the negative stiffness element. Based on this model, when κ_1 is tuned to be more negative gradually from -3.3334 to $-3.36\,\mathrm{kN/m}$, the resonance-like peak shifts to relatively higher frequency regimes, but if κ_1 is too negative (less than $-3.36\,\mathrm{kN/m}$), the peak moves back toward low frequency regimes, and eventually, becomes a hump again (for example, $\kappa_1 = -4\,\mathrm{kN/m}$). Moreover, around 1 rad/s, the peak with $\kappa_1 = -3.34$ coincides with the peak with $\kappa_1 = -3.744\,\mathrm{kN/m}$. But, the latter has a 100 times greater divergent rate.

In figure 6(b), the magnitude of the effective dynamic spring constant ($|k^*_{\mathrm{eff}}|$) is plotted versus frequency (0.01 to 100 rad/s). As can been seen, far away from the stability boundary (for example, $\kappa_1 = -3.091\,\mathrm{kN/m}$) in the stable regime, the frequency dependence of $|k^*_{\mathrm{eff}}|$ is small. From that, the frequency dependence becomes stronger up to $\kappa_1 = -3.3333\,\mathrm{kN/m}$. When approaching the stability boundary, $|k^*_{\mathrm{eff}}|$ becomes $2 \sim 3$ orders of magnitude larger in the frequency range of 10 to 100 rad/s than in that of 0.01 to 0.1 rad/s.

When κ_1 is so negative that the system becomes metastable, for example $\kappa_1 = -3.34\,\mathrm{kN/m}$, the frequency dependence of $|k^*_{\mathrm{eff}}|$ is reduced. For even more negative κ_1 ($\kappa_1 = -3.74\,\mathrm{kN/m}$), one observes an anomalous dispersion in which $|k^*_{\mathrm{eff}}|$ need not increase with frequency. In this regime the system is unstable. Very strong negativity in κ_1 ($\kappa_1 = -4\,\mathrm{kN/m}$) reduces the reversed frequency dependence of $|k^*_{\mathrm{eff}}|$. It is noted that, from figure 5, with positive κ_1 at 1 rad/s, the magnitude of the effective dynamic spring constant is about $3\,\mathrm{kN/m}$.

As for extremely high $\tan\delta$, we remark (figure 6a) that for $\kappa_1 > -3.3333\,\mathrm{kN/m}$, one can obtain a stable $\tan\delta$ of 1 to 100 (approaching 1000 when very close to the stability boundary) at low frequency. This is higher than that of commercial high damping rubbers ($\tan\delta \sim 1$). However, at low frequency, the system has a low stiffness near the stability boundary. Physically the peaks in attenuation arise from the fact that point m_1 moves much more than the driven point m_2. The proper balance between positive and negative stiffness causes an amplification of motion.

As for resonance-like singular peaks in $\tan\delta$, the phenomenon is in principle observable near the stability boundary. Specifically, for the peak close to the stability boundary in the metastable regime, e.g. $\kappa_1 = -3.3334\,\mathrm{kN/m}$, the time constant for divergence is 667 seconds, and the required time period for experimental observation of five cycles at the peak's frequency 0.07 Hz is only about 70 seconds. The observability, therefore, may be achieved by tuning parameters such that the driving frequency is much greater than the stability-losing eigenvalue. Singular peaks in $\tan\delta$ are not observable if the system contains such high negative stiffness that the time constant for divergence and the period of driving force are comparable. For instance, the $\tan\delta$ peak for $\kappa_1 = -3.744\,\mathrm{kN/m}$ has the time constant for divergence

about 0.1 seconds, but it takes about 6.28 seconds to complete a cycle of the applied sinusoidal driving force. Under these conditions, it is not observable.

As for possible experimental observations, we recall that large peaks in $\tan\delta$ of systems with a negative stiffness constituent were reported by (Lakes 2001a, Lakes *et al.* 2001) as a function of pre-strain or temperature. Frequency tuning was not done in these studies, and the distinction between stable and metastable behaviour was not explored. These results reveal the role of negative stiffness in systems more complex than the one in the present analysis. The present model system generates negative stiffness based on geometrical nonlinearity. While it does not contain explicit temperature dependence, one may draw correspondences with crystals which undergo phase transformation. For such crystals, a snap-through effect similar to that described here occurs as temperature changes, by virtue of the effect of temperature on interatomic bonds. For the present model to represent such crystals, the negative stiffness becomes a function of temperature as well as strain. For materials with a single mechanism for viscoelastic response, there is an Arrhenius relationship between temperature and frequency. In that context, the frequency dependence analysed here can be interpreted in the context of temperature dependence. As for observed damping in alloys, broadband damping $\tan\delta$ observed in indium-tin alloy by Lakes and Quackenbush (1996) followed a power law ν^{-n} over many decades of frequency ν. Since $n = 0.28 < 1$, the observations cannot be explained by a simple model.

The implication of the resonance-like peaks is provocative. For example, atomistic models of grain boundaries (Alber *et al.* 1992, Bassani *et al.* 1992) disclose metastable or unstable phases which lose positive definiteness or strong ellipticity, hence have negative moduli. In this context, physical ageing in crystalline materials may provide a flux of 'new' material converted to metastable form. While experiments intentionally designed to reveal effects due to these metastable boundaries have not yet been reported, it is possible such effects have been observed. For example, Fitzgerald (1957, 1966) reported resonance-like dispersion below any known natural frequency in several polycrystalline metals. These peaks were eliminated by annealing. Similar dispersion effects were reported by Pugh *et al.* (1973) in human bone which has hierarchical structure (Lakes 1993b). Since the quantum mechanical mechanism suggested was not generally accepted, we consider metastable phases as an alternative mechanism worthy of further study.

§ 4. Conclusions

The damping, $\tan\delta$, of discrete viscoelastic systems can be greatly magnified by incorporation of a negative stiffness element. The high damping occurs as a broad low-frequency peak in stable systems, and as a sharp singular peak in metastable or unstable systems. The singularity resembles a resonance but occurs in the quasi-static regime far below any natural frequency. The system can exhibit stiffness greater than that of any constituent in the metastable regime.

Acknowledgments

We thank the NSF for support via grant CMS-0136986. Many useful discussions with W. Drugan are gratefully acknowledged.

References

Alber, I., Bassani, J. L., Khantha, M., Vitek, V., and Wang, G. J., 1992, *Phil. Trans. R. Soc.* A, **339**, 555.

Bassani, J. L., Vitek, V., and Alber, I., 1992, *Acta metall. mater.*, **40**, S307.

Bathe, K. J., 1996, *Finite Element Procedures* (Englewood Cliffs, New Jersey: Prentice Hall).

Bramble, J. H., and Payne, L. E., 1963, Proceeding of the Fourth National Congress of Applied Mechanics, pp. 469–473.

Dorf, R. C., 1992, *Modern Control Systems*, eighth edition (New York: Addison-Wesley).

Fitzgerald, E., 1957, *Phys. Rev.*, **108**, 690.

Fitzgerald, E., 1966, *J. acoust. Soc. Am.*, **39**, 870.

Hashin, Z., and Shtrikman, S., 1963, *J. Mech. Phys. Solids*, **11**, 127.

Iesan, D., 1989, *Pre-stressed Bodies* (Longman Scientific & Technical).

Knowles, J. K., and Sternberg, E., 1978, *J. Elasticity*, **8**, 329.

Lakes, R. S., 1987, *Science*, **235**, 1038; 1993a, *Adv. Mater.*, **5**, 293; 1993b, *Nature*, **361**, 511; 2001a, *Phil. Mag. Lett.*, **81**, 95; 2001b, *Phys. Rev. Lett.*, **86**, 2897.

Lakes, R. S., and Drugan, W. J., 2002, *J. Mech. Phys. Solids*, **50**, 979.

Lakes, R. S., Lee, T., Bersie, A., and Wang, Y. C., 2001, *Nature*, **410**, 565.

Lakes, R. S., and Quackenbush, J., 1996, *Phil. Mag. Lett.*, **74**, 227.

Leipholz, H., 1980, *Stability of Elastic Systems* (Alphen aan den Rijn, The Netherlands: Sijthoff ans Noordhoff); 1987, *Stability Theory* (New York: John Wiley & Sons).

Meirovitch, L., 1970, *Methods of Analytical Dynamics* (New York: McGraw-Hill).

Paul, B., 1960, *Trans. AIME*, **218**, 36.

Pugh, J. W., Rose, R. M., Paul, I. L., and Radin, E. L., 1973, *Science*, **181**, 271.

Strogatz, S. H., 1994, *Nonlinear Dynamics and Chaos* (Cambridge, Massachusetts: Perseus Books).

Wang, Y. C., and Lakes, R. S., 2001, *J. appl. Phys.*, **90**, 6458; 2003, *Q. appl. Math.* (to be published); 2004a, *Am. J. Phys.*, **72**, 40; 2004b, *Appl. Phys. Lett.*, **84**, 4451.

Zener, C., 1948, *Elasticity and Anelasticity of Metals* (Chicago, Illinois: The University of Chicago Press).